A novel enhancing LVRT capability of DFIG based wind turbine systems

J.MOHAMMED FEROS KHAN[1*], Dr.N.SHANMUGA VADIVOO[2],
[*1]*Assistant Professor, Department of EEE,Vickram College of Engineering,feros.jj@gmail.com,*
[2] *Assistant Professor, Department of EEE,Thiagarajar College of Engineering ,nsveee@tce.edu,Madurai, India.*

Abstract-In recent decades, concerns regarding carbon emissions, climate change, and limitation of fossil fuels have led to a large increase in generation of electricity via renewable resources. Wind energy has been one of the more successful of these new additions to the generation pool. In this work, doubly fed induction generators (DFIGs) are employed in the wind generation systems. The 3-phase power produced from the wind turbines is given in a grid by means of a suitable interfacing device. Normally the wind power systems are affected by environmental discrepancies and fault disturbances occurred at the transmission level. Hence a Fault Ride Through (FRT) system is employed in the wind power systems to prevent the disconnection of wind farm even under the fault condition. Typically the. A Low Voltage Ride Through (LVRT) is essential with a higher degree of control becauese transmission line undergoes an abrupt change of the fault. Here a nonlinear control system is employed to face the abrupt changes of the voltage and to maintain the system to be stable without a damping system. In this work, a fuzzy controlled active ride through control based on the parallel resonance fault current limiter is presented to obtain the best performance in the FRT systems. The parallel resonance type fault current limiter (PRFCL) is a new auxiliary device manifesting potential application in power systems, which can be simply controlled by determining the proper switching schemes. In order to validate the effectiveness of the parallel resonant filter, a MATLAB/Simulink model has been built and the system is studied with fuzzy controller and compared to the active crowbar circuits. In that the resonant current filter provides a more effective voltage control, i.e. the voltage stability of the line increases. It is observed that the proposed Fuzzy Logic control-parallel resonance type fault current limiter (FLC-PRFCL) seems to be efficient for augmenting the ability of FRT of the DFIG based wind farm. Moreover, the proposed FLC-PRFCL outperforms the crowbar.

Keywords- Fault Ride Through (FRT), Low Voltage Ride Through (LVRT), Doubly fed induction generators (DFIG), reactive power, Wind turbine

1. Introduction

Wind power generation has become one of the most commercially usable alternative renewable sources now a days. As penetration of wind energy has reached a substantial level, new power system operation issues have arisen as well. According to the new operational strategies, the wind firms must be continuously connected to the grid without any interruption and provide reactive power for supporting the grid voltage during the grid faults [1]. This capacity of wind firms is known as the fault ride through (FRT) capability and also as the low voltage ride through (LVRT) capability. Now, DFIG is generally used for wind turbines as it has several advantages like variable speed constant frequency based operation, decoupled control of active and reactive power and partial-scale converters.

The most imperative concerns related toworking of wind farms in the presence of low voltage faults are the low voltage event performance of hybrid wind farms containing economical Fixed Speed Induction Generators (FSIGs) and the most commonly used Doubly-Fed Induction Generators (DFIGs).On the occurrence of fault in the network, the voltage drop producesadverse effects on wind turbines. Hence a power loss occurs in active power and the system requires more difficult techniques to resolve the low voltage event. This event directs the network administrators and controlling agencies to LVRT capability requirements on wind farms. Though the features are different for different networks, LVRT requirements identify worst-case fault events such as % drop in voltage,duration, and recovery time. The adjustments in devices and functions cause large variations in LVRT based on the type of turbines employed in the wind power system. The two major components of the wind turbine that can be regulated are the blades (e.g. pitch

angle) and the generator. This paper explains LVRT with two types of generators and performance of the system is observed based on the generator types and their controls, instead of considering the pitch angle control.

A vector-based current control method was presented in recent days to obtain fast transient response in the DFIG. When the entire models of the DFIG machine and the corresponding control system are developed in the PSCAD power systems simulation software, some consequences are simulated and scrutinized effectively to detect the confines associated with the practical capabilities of DFIG Precisely, the maximum ratio of FSIG to DFIG along with the factors affecting this ratio like DFIG rotor current and FSIG over-speed relays are examined. The main aim of this paper is to obtain reduced total cost in a hybrid wind farm. When the FSIG systems are used, the drop in terminal voltage in the case of fault produces a drop in the electromagnetic torque of the machine. A power/torque mismatch happens because of the constant mechanical input (Wind speed) and hence the rotor rapidly accelerates. The fault must be rectified quickly otherwise the rotor acceleration cannot be stabilized and will accelerate unceasingly even the fault is rectified. In order to avoid the mechanical damages in the system, the over-speed relays will trip to separate the machine from the network. Moreover, FSIG reactive power consumption becomes high during faults and the network requires a more difficult method to rectify the problems.

Nowadays, the wind power generation system and the LVRT regulations have forced to many research on LVRT schemes. The most common solution for FSIG wind farms includes some FACTS (Flexible AC Transmission System) devices for quick reactive power compensation during faults. These devices are switched capacitors, static VAR compensators (SVCs), and STATCOMs (Static Compensators) [2-4]. They are installed at the wind farm location and they are activated during fault detection in order to inject a certain amount of reactive power for maintaining the stable condition and the connection of the wind farm.

DFIGs operate in a different manner during faults, and hence their LVRT concerns and solutions are also different. When a fault occurs on the network, locating nearer to a DFIG, the modification in stator flux affects the rotor windings and hence the rotor current increases beyond therated current. The general solution for this problem isa ‘crowbar’ which short circuits therotor windings in order toavoid excessive currents [5-7]. However, this disconnects the wind firm from the grid and therefore the crowbar is not suitable for LVRT. FACTS devices can be employed with DFIGs in the same manner how they are employed with FSIG.

Now, many research works havebeen accomplished which proposed the utilization of conventional control methods in the rotor-side converter (RSC) and grid-side converter (GSC) of the DFIG to obtain various operations. In these control methods, a main concern is regarding the targeted functionality whether it works during steady state or transients. Particularly, those control methods focusing on attaining successful transient performance during a fault,exhibit difficulties in obtaining fast response. The reason behind this is that the control methods depend onthe real-time measurement of the stator flux and it is tough to obtain.

This paper considers the hybrid wind farms containing FSIGs and DFIGs and examines the DFIGs' reactive power control ability to offer LVRT for the nearest FSIGs. The developed transient response of the controller is utilized to let the DFIGs to add reactive power on the occurrence of fault and. Conversely, in this work only the rotor-side converter takes part in reactive power injection and disregards the capability of the grid side converter. Moreover, this work focuses only the system with a large ratio of DFIGs to FSIGs.

In this work, a fuzzy controlled active ride through controlled based on the parallel resonance fault current limiter is presented to obtain the best performance in the FRT systems. The parallel resonance type fault current limiter (PRFCL) is a new auxiliary device manifesting potential application in power systems, which can be simply controlled by determining the proper switching schemes. In order

to validate the effectiveness of the parallel resonant filter, a MATLAB/Simulink model has been built and the system is studied with fuzzy controller and compared to the active crow bar circuits.

2. Literature survey

Recently the modified control strategies are reported as the mostefficient method for FRT scheme. In these control methods, the control structure is reformed rather than employing more hardware components. In literatures [8] and [9], the RSC outputs voltage is increased and the rotor over current is decreased by introducing the stator voltage feed-forward compensation methods in the output side of the RSC current controller. In paper [10], the stator current is taken as the rotor current reference in the event of grid faults and which makes the stator and rotor over current to become low. In [11], the gain of the PI current controller of rotor sideis changed to reduce the rotor over currents and increase the flux attenuation. In paper [12], the FRT control method is proposed in which a nonlinear control method isgiven to the RSC and a DC-link voltage control given to the GSC. This method makes damping of the DFIG transient response to be better and reduce the oscillations of the rotorcurrent, electro magnetic torque and DC-link voltage in the case ofgrid faults.In [13], a control method based onthe instantaneous rotor power feedback is proposed which controls the voltage fluctuation happened at the DC-link. In work [14], nonlinear control strategy is applied to the GSC to damp out the internal dynamicsand to reduce the DC-link voltage fluctuations. Wang et al [15] presented a coordinated control strategy by using the grid side controller as the main source for controlling the reactive power and the rotor side converter as the auxiliary source for reactive power control and to support the grid voltage recovery.These works [8-15] providegood results forthe symmetrical type of faults. However, most of the gird faults are of asymmetrical type. Similarly, these methods can improve the FRT capability when the voltage sags are moderate and they fail to reduce the rotor currents when the voltage sags are deep. In paper[16], the authors introduced a method which merges the crowbar and the utilization of demagnetizing currents to enhance the FRT capability during deep sags. However, this method has a disadvantage that the RSC control scheme is deactivated temporarily when the crowbar is activated and hence the DFIG drawsreactive power from the grid.

In paper [16], the authors utilized DFIG to improve the transient stability of the squirrel cage induction generator. But in this method two-mass drive train model of wind turbine generator system (WTGS)[17] is not taken into account and it shows a substantial effect on the transient stability of the fixed speed WTGS. Muyeen et al [18]used a permanent magnet synchronous generator(PMSG) based variable speed wind turbine (VSWT) with the fixed speed WTGS to regulate the reactive power and to supply maximum power to the grid. In this work a multilevel-based frequency converter is used to connect the VSWT generation system with the power system in order to obtain better harmonic performance.Literature [19], studied the stability of traditional synchronous generators and wind turbines based on DFIG

3. Wind turbine generator model

The basic structure of the DFIG is depicted in figure 1.The DFIG is joined to the point of common coupling (PCC) with the stator and the rotor. The stator is joined to the PCC directly, whereas the rotor is connected by means of the variable frequency converters. The rotor also employs a back-to-back converter toregulate both active and reactive power. A low-speed shaft, a high-speedshaft with agearbox is placed in between thewindturbineand the DFIG A crowbar is placed between the RSC and DFIG in order to protect the RSC from the damage occurred in the transient condition.

3.1 Wind Turbine Aerodynamics Model

The output power taken from the wind turbine is

$$P_m = \frac{1}{2}\rho A C_p(\lambda,\beta)v^3 \quad (1)$$

Where, $\lambda = \frac{\omega_m R}{V}$ (2)

where, ρ is air density, A is cross-sectional area of the turbine ($m^{2)}$, C_p (λ, β) is Wind turbine power

coefficient, which is the function of pinch angle β (in degrees) and tip-speed ratio λ (as given in Equation (2)),*v* is the wind speed (m/s) [22]. $\omega_m$is shaft speed and *R* is radius of the blades.

3.2 Control of the RSC

The active power and reactive power of the stator can be split by utilizing thenotion behind the stator-flux-associated reference structure to the RSC.Therefore, the voltage control of the RSC has two serially connected control loops as shown in

Figure1.The output control loop provides d-axis reference current $i_{dr}^*$and q- axis reference current i_{qr}^* to adjust the current in theinner-loop.

3.3 Control of the GSC

The grid-side converter controls the DC voltage and the reactive power balance between the grid and the grid side converter with the help of a vector control applied to grid voltage. The voltage control of GSC alsohas two serially connected control loops. The output generated reference signals i_{dr} and i_{qr} are for inner-loop current regulation.

3.4 DFIG capability limits

The capability of the DFIG have several limits on stator androtor. The equation of the stator sideis given in eqn (3).

$$P_s + Q_s = 3U_s^2 I_s^2 \quad (3)$$

where P_s is active power,Q_s is reactive power, U_s is rated voltage (in p.u) and I_s is rated current (in p.u) respectively.

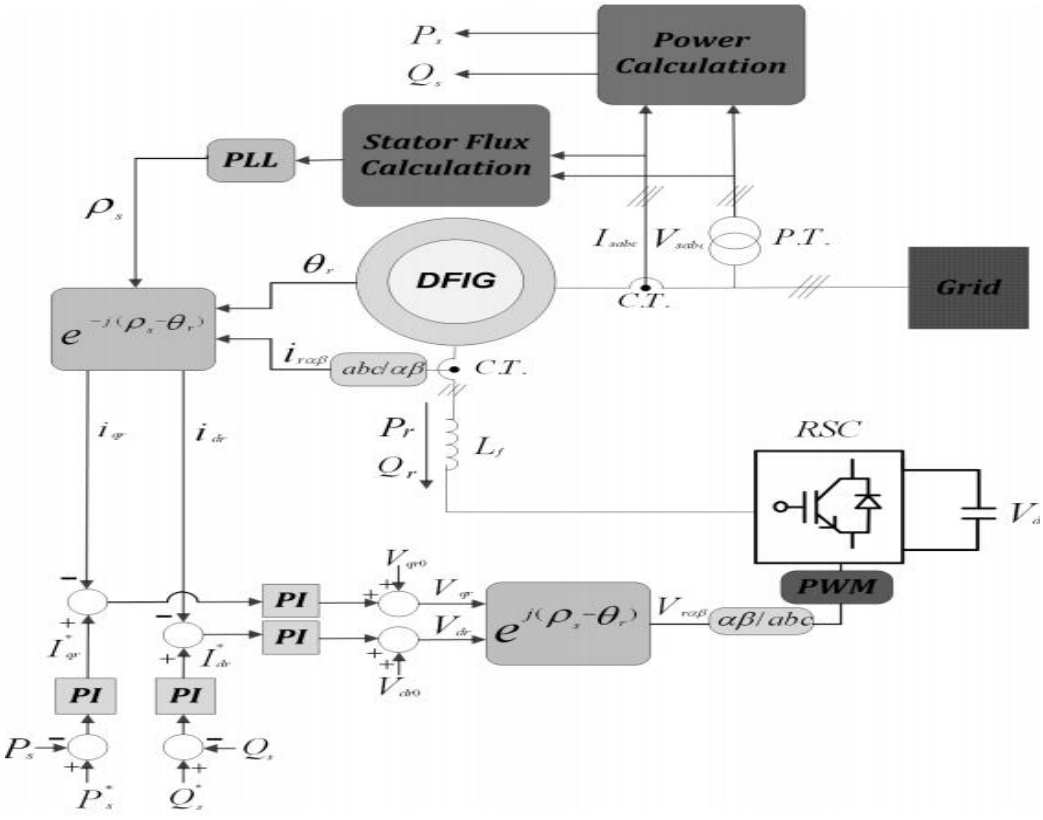

Figure 1. Voltage Control of the RSC

According to Joule's law the stator active power ad reactive power in at rated voltage are given in Equation (4) and (5).

$$P_s = 3\frac{X_m}{X_s} U_s I_r \sin\theta \quad (4)$$

$$Q_s = 3\frac{X_m}{X_s} U_s I_r \cos\theta - \frac{U_s^2}{X_s} \quad (5)$$

From Equation (4) and (5), Equation (6) is obtained.

$$P_s^2 + \left(Q_s + 3\frac{U_s^2}{X_s}\right)^2 = 3\frac{X_m}{X_s} U_s I_r \quad (6)$$

Hence, in PQ plane rotor boundaryis obtainedwith the center of $\left[3\frac{U_s^2}{X_s}, o\right]$ and radius of $\left(3\frac{X_m}{X_s} U_s I_r\right)^{\frac{1}{2}}$ is obtained.

3.5 Drive train

In this work, two mass shaft model taken for the dynamic analysis of grid connected wind turbines as depicted in Figure 2.

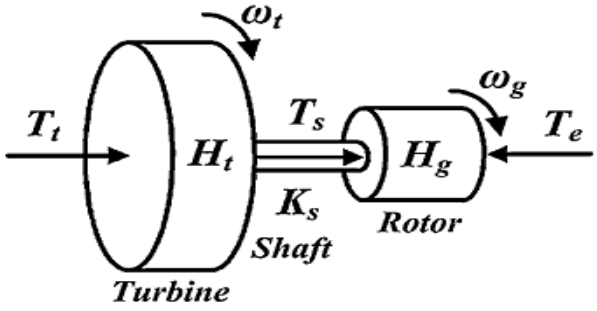

Figure 2. Drive train

The motion equations are given in Equations (7), (8) and (9).

$$\frac{d\theta_s}{dt} = \omega_t - \omega_g \quad (7)$$

$$\frac{d\omega_t}{dt} = \frac{1}{2H_t}(T_t - K_s\theta_s) \quad (8)$$

$$\frac{d\omega_g}{dt} = \frac{1}{2H_g}(-T_e + K_s\theta_s) \quad (9)$$

whereT_t is the mechanical torque with reference to the generator side, T_e is the electromagnetic torque, ω_t is the turbine rotational speed,ω_g is the generator rotational speed,K_s is the shaft stiffness, H_t is the equivalent turbine-blade inertia referred to the generator side,$H_g$is the generator inertia,and θ_s is the angular displacement between the end soft he shaft.

3.6 DFIG modeling

The DFIG is designed using the Park's transformation model.Here, ad–q reference frame revolving at synchronous speed is selected.It is assumed that the stator flux comes in line with the d-axis. Hence the stator flux and the reference frame revolve at the same speed.This choice enables the decoupled control of the generator electrical torque and the rotor excitation current.

3.7 RSC controller

The rotor side and grid side converters are same and designed as 2-level,3-phase full bridge converters using insulated gate bipolar transistors (IGBT) switches. Depending on the reactive power Q_t, the generator terminal voltage V_t, and the generator speed ω_r, the RS Controller controls the active and reactive power output as shown in Figure 3.The proportional-integral(PI) controller provides the reference signal for the pulse width modulation (PWM) block. The PWM block then produces appropriate signals for the IGBT switches that made up the RSC. In order to reduce controller complexity, linear control technique is adopted over non linear and more complex controllers.

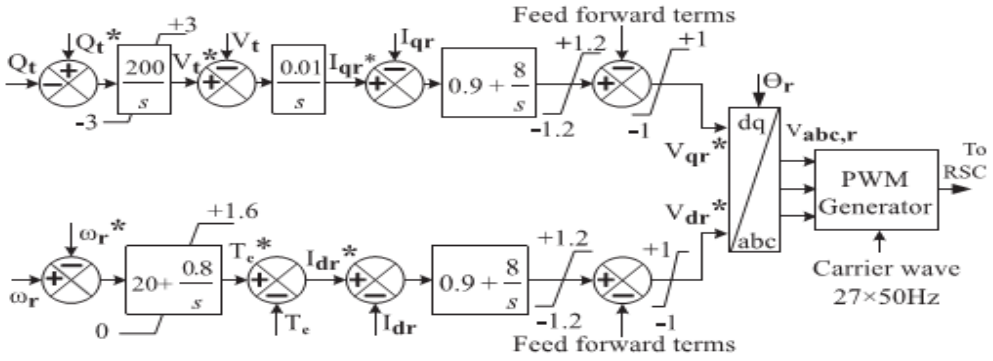

Figure 3. RSC controller

3.8 GSC controller

The GSC controller in Figure 4, takes the dc-link voltage Edc and the grid side quadrature currentI_q gas the inputs.The PI controllers then produce necessary reference signals to control the IGBT switches at the GSC. A constant dc-link voltage and system required power factor at the generator terminal are ensured by the GSC controller. The frequency of the carrier waves used in the PWM blocks of both the RS C and the GSC controllers is chosen to abate the harmonics.

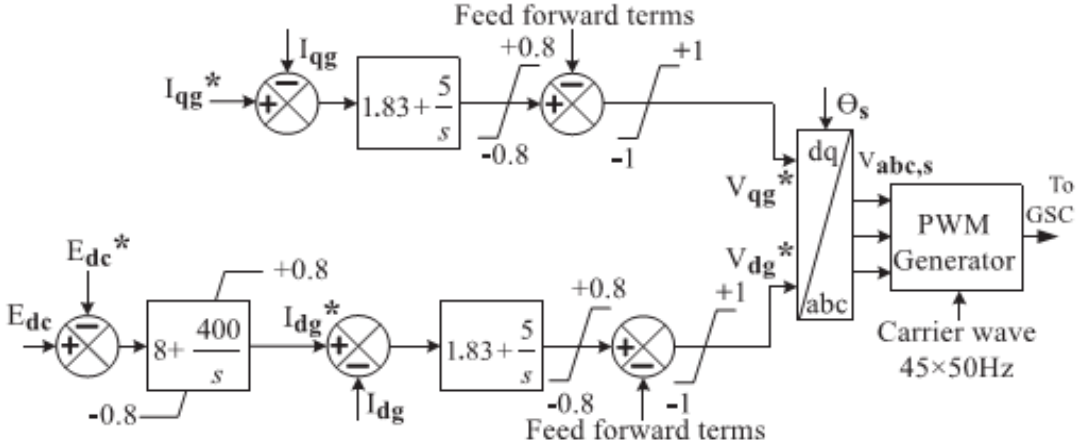

Figure 4. GSC controller.

4 Fuzzy logic controlled PRFCL

The modeling of the proposed FLC-PRFCL is described as follows.

4.1 PRFCL configuration

The per phase diagram of the PRFCL is shown in Figure5. The topology comprised of two distinct parts.These parts are described as follows.

1.Bridge part: Four diodes D_1–D_4, arranged in bridge formation, build the bridge part. In the diode bridge, an IGBT switch in series with a dc reactor LDC is placed.Depending on system requirements, series/parallel combination of IGBTs can be used. The inherent resistance of the dc reactor is considered by placing a very small value resistor $R_{d,}$ C_{in} series with the dc reactor.The free wheeling diode D_5 ensures safe operation of the dc reactor LDC.

2.Resonance part: The shunt resonance part is comprised of a capacitor C_{sh} and an inductor lies arranged in parallel to each other to form an LC resonant circuit at power line frequency.

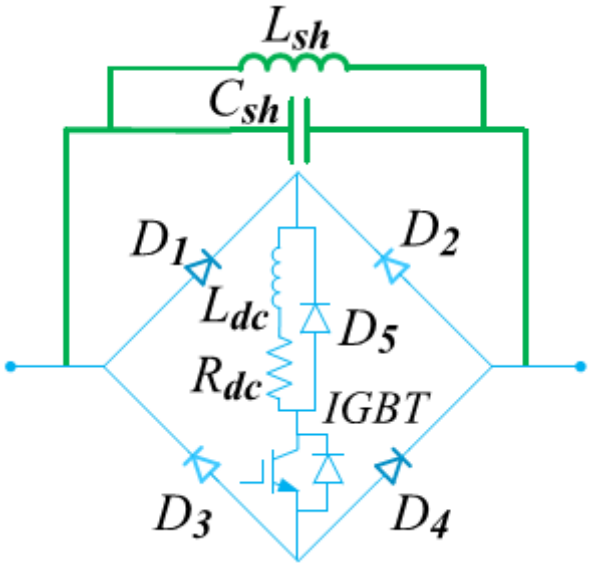

Figure 5. Per phase diagram of PRFCL

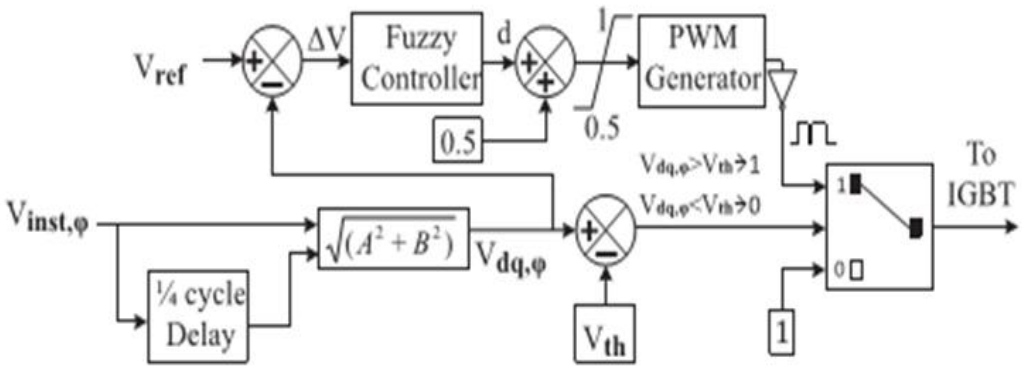

Figure 6. Per phase fuzzy logic based controller for PRFCL

4.1.1 PRFCL operation and control

When the system is in normal operation, the IGBT switch stays closed and carries the line current fully. For the positive and negative half cycle of voltage, the D_1–L_{dc}–R_{dc}–D_4 path and D_2–L_{dc}–R_{dc}–D_3 path carries the line current.But current going into the dc reactor L_{dc}, is from the same direction. So current flowing into the dc reactor L_{dc} is dc current. L_{dc} is charged up to the peak value of current and the current ripples are smoothed out by it. The turn on the resistance of the IGBT, Rdc, and forward voltage of diode altogether cause some voltage drop. In comparison to the line voltage drop,this voltage drop is ignorable and has an insignificant effect on normal operation. The shunt path impedance is high enough so that the bridge path conducts the line current entirely, except very small leakage current through the shunt path. When faults occur, the line current rise rapidly,but the rate of change di/dt, is suppressed by the dc reactor L_{dc}.This ensures the safe operation of the IGBT. The per phase controller for the PRFCL is shown in Figure6.

The instantaneous phase voltage of the wind turbine, which is denoted as $V_{inst,\phi}$ or $V_{d,\phi}$ is obtained and the delay of ¼th cycle is given to generate a quadrature counter part$V_{q,\phi}$. Then $V_{dq,\phi}$ is generated as $V_{dq,\phi}= (V^2_{d,\phi}+V^2_{q,\phi})$. The difference between $V_{dq,\phi}$ and the reference voltage V_{ref} is obtained and it is denoted as V which is applied to the FLC. The FLC output is varied to obtain adutyratio in the range of 0.5 to 1. It ensures that very small impedance is not connected in the event of the fault. The occurrence of fault is detected by comparing the threshold voltage level which is equal to 0.9 p.u with the voltage $V_{dq,\phi}$.When the threshold voltage is less than $V_{dq,\ \phi}$ (normal operation) a signal value of 1 is applied to the IGBT and to the inverted PWM generator output when threshold voltage is greater than $V_{dq,\phi}$. The modified voltage $V_{dq,\phi}$ enables quick fault detection. The best compensation is obtained by applying a variable shunt impedance value (Z_{sh}) instead of a full value throughout the fourth period. The variable impedance value is obtained as Z_{sh}=d∗Z_{sh}.The duty ratio, d isproduced by the FCL. The dutyratio,disdefinedas

$$d = \frac{T_{off}}{T_c} \qquad (10)$$

Where T_c is the time period of the carrier signal applied to the PWM generator which is the sum of two time periods (T_{off} and T_{on}), T_{off} is the time period during which the NC-MBFCL bridge IGBT does not conduct. T_{on} is the time period during which the NC-MBFCL bridge IGBTconducts and f_c(=1/T_c) is the carrier wave frequency of the PWM generator. The variable shunt impedance enables the FLC-PRFCL to dynamically react to the various levels of the faults.

4.2 Fuzzy logic controller design

Fuzzy control was presented by to establish a controller based on human knowledge.Basically, an FLC consists of three main modules: the fuzzification process, theinference engine and the defuzzification process. Fuzzification maps inputs from crisp values to linguistic values and defuzzification has the reverse role in a fuzzy system.The FLC acts properly when appropriate knowledge of a system is applied to its design. Since the reactive power demand is computed from the voltage value and its derivative, the setwofactors are given as inputs to the FLC. Likewise, the output signal must be interms of reference values for reactive power and active power amplification factors. The rule base is kernel part of an FLC. According to Figure 5, the reference reactive power needs to be maximized in conditions of a drop in voltage of more than 50% and take a value appropriate to the conditions of that drop in voltage. The active power must be reduced to assign a proper value to reference active power. Hence, as the reference reactive power gets a higher value, the active power must get a lower value.Thus, rules can be determined as represented in Tables 1.

The fuzzy controller designed to control the FLC-PRFCL is delineated below. The difference between the reference voltage and the wind farm terminal voltage,V, and the duty cycle, dof the PWM generator block atFigure6,are chosen as the input and the output, respectively, for the design of the proposed fuzzy logic controller. Gaussian member ship functions (MFs) for Vanddareshown in Figs.7 and 4.8, in which the linguistic variables ZE,SM,HI,MB, and BI stand for zero, small medium, high, medium big and big, respectively. Other types of MFs, for example, the triangular and the trapezoidal MFs were also tried in Matlab, but Gaussian MFs gave the best performance. Also, some adjustments were do netothe Gaussian MFs to get the best system performance. The equation of the Gaussian MFs[22] used to determine the grade of membership values is as follows:

$$f(x;\sigma,c) = e^{-\frac{(x-c)^2}{2\sigma^2}} \qquad (11)$$

whereσandcdefinesthewidthofthebellcurveandthecenterof the peak,respectively.

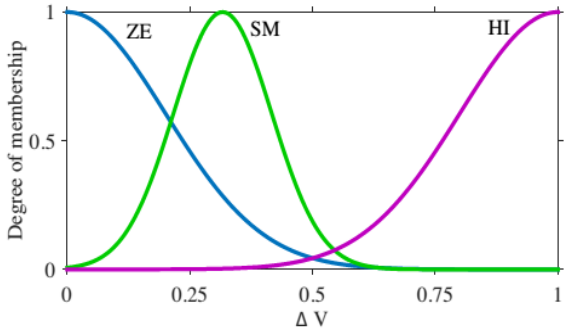

Figure 7. Membership function of input V

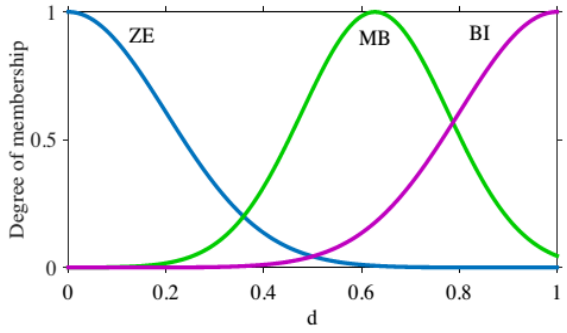

Figure 8. Membership function of output d

The very simplede sign having only one input variable and one output variable is the specific feature of the proposed fuzzy controller. The use of single input and single out put variable makes the fuzzy controller very straight forward[23].Table 1 depicts the control rules of the FLC, which are derived from the perspective of system process, and they facilitate the improved system performance.

Table 1 Fuzzy rule table

PCC Voltage deviation, ΔV	**Duty cycle, d**
ZE	ZE
SM	MB
HI	BI

Mamdani's method is used for the inference mechanism that gives the degree of conformity,Wi,of each fuzzy rule as follows:

$$W_i = \mu_i(\Delta V) \qquad (12)$$

Where *i* is rule number.

4.2.1 Defuzzification

The center of gravity procedure is a well-known Defuzzification procedure. This is implemented to determine the output crispy value (i.e.,thedutycycle,d), given by the expression below,

$$d = \frac{\int z\mu_i(z)dz}{\int \mu_i(z)dz} \qquad (13)$$

whereμi (z) is the value of dexpressed interms of linguistic variables in the fuzzy rule table.

4.2.2.Influence of operating point on FLC

When the changes happened in the speed of the wind, the proposed FLC operation will be affected.Hence the control parameters of the FLC must be altered in response to the changes in the speed. However,in this work since we are dealing with fault or transient situations,it is assumed that the wind speed is constant during the short time period under consideration and hence only one set of fuzzy control parameters are used to show the effectiveness of the proposed work.Certainly, the fuzzy parameters are well tuned so that they can work well for both balanced and unbalanced fault conditions.

4.3. PRFCL design considerations

A consolidated average model of IGBT is considered in thiswork which can withstand system operation. The PRFCL computes the suitable values of the shunt capacitance,C_{sh} andinductance, L_{sh}.The pairs of C_{sh} and L_{sh} values would providers on an ceat power frequency. But typical values of C_{sh} are selected from[32] and L_{sh} value is computed based on the resonance at power frequency. Different resonating pairs of C_{sh} and L_{sh} values were taken for analysis. Among the explored pairs,C_{sh}=300F and L_{sh}=38mH were observed as the pairs to provide the best performance under fault conditions.

4.3.1. PRFCL with proportional-integral (PI) control

To compare the performance of the proposed FLC-PRFCL with a simple yet use ful controller, the proportional-integral(PI)control has been chosen. The topology of the controller is showninFigure9. To keep the comparison fair and reasonable, only the fuzzy controller portion of Figure 6 is replaced with a PI control block. The control parameters were adjusted for optimal system performance, and it was found that the proportional gain of 0.7 and integral gain of 0.75 yield the optimum system performance.

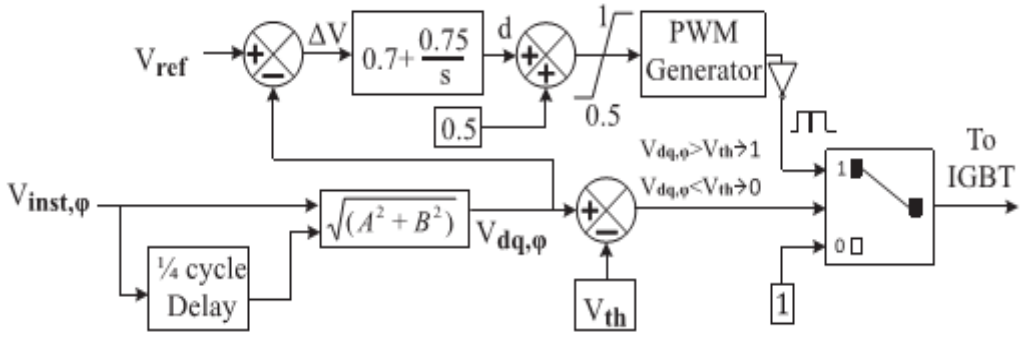

Figure 9. Per phase proportional-integral (PI) controller for PRFCL.

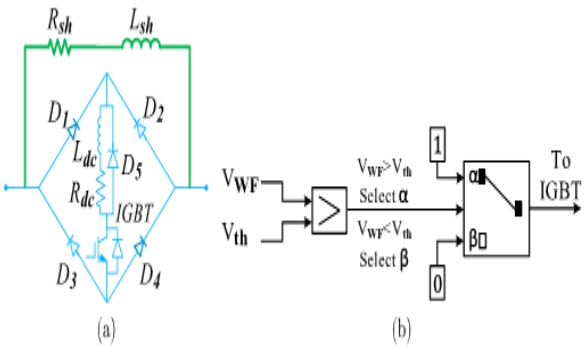

Figure 10. Per phase (a) topology of BFCL and (b) BFCL controller

4.4. Bridge-type fault current limiter

In order to see the efficacy of the proposed FLC-PRFCL, its performance is compared with that of the BFCL. Both the BFCL and the PRFCL share the same bridge part, but the difference is in the shunt path. In the BFCL, a series connected resistor and inductor is employed as the shunt path impedance which is depicted inFigure10a. The working process and control methodology of FCL is same as in the PRFCL. Similarly, the BFCL is connected at the same place where the PRFCL was connected. The BFCL controller is given in Figure10b. The RMS voltage at the point of common coupling (PCC) or the wind farm terminal (V_{WF}) is used to detect faults by comparing with a preset threshold voltage V_{th}. When$V_{WF}>V_{th}$, the IGBTs are turned on and when $V_{WF}<V_{th}$, a fault is detected and IGBTs are turned off to by pass the fault current to the shunt path.

The condition for designing BFCL requires that the shunt path of the BFCL simulates the load impedance to the wind farm. The wind farm is connected to the transmission system, where the impedance does not change that much compared to that of a distribution system. This makes the construction of the BFCL simple. The values of the R_{sh} and L_{sh} are determined by measuring the impedance seen from PCC and using the techniques described in[3]. The values R_{sh}=4.2 and L_{sh}=0.1168mH are used in this work.

5 RESULT AND DISCUSSION

A fuzzy logic controlled -parallel resonance fault current limiter (FLC-PRFCL) is proposed to aid the DFIG based wind farms to achieve improved FRT capability. To assess the performance of the proposed FLC-PRFCL, symmetric and asymmetric faults were momentarilyapplied to the multi-machine system, to which a DFIG based wind farm is connected. The experimental results obtained for the proposed FLC-PRFCL are compared with the results of bridge-type fault current limiter (BFCL) and conventional proportional-integral (PI) control based PRFCL (PI-PRFCL).The proposed Fuzzy based LVRT scheme is evaluated in MATLAB SIMULINK model. In order to perform experimental validation, a DFIG wind turbine generating power at 575V is used. A grid side controller is connected with it. The output of the wind turbine is stepped up using 575V/34.5kV step up transformer and fed into a 55 km transmission line. The 2-phase and 3-phase LL faults occurring on the transmission line are considered. The performance of the system under these faults is evaluated for different scenarios. The performance is

evaluated without LVRT system, with LVRT system and with LVRT-Fuzzy system. The corresponding Simulink diagram and the output waveforms are shown in the figures below. The simulation waveform output of each simulation consists of six different waveforms. They indicate DFIG output voltage, Bus voltage, Angular speed, Electrical output, D-axis variations and Q-axis variations respectively. Figure11 shows the simulation of the system under 2-phase fault, without LVRT system and the respective waveform is shown in Figure 12.

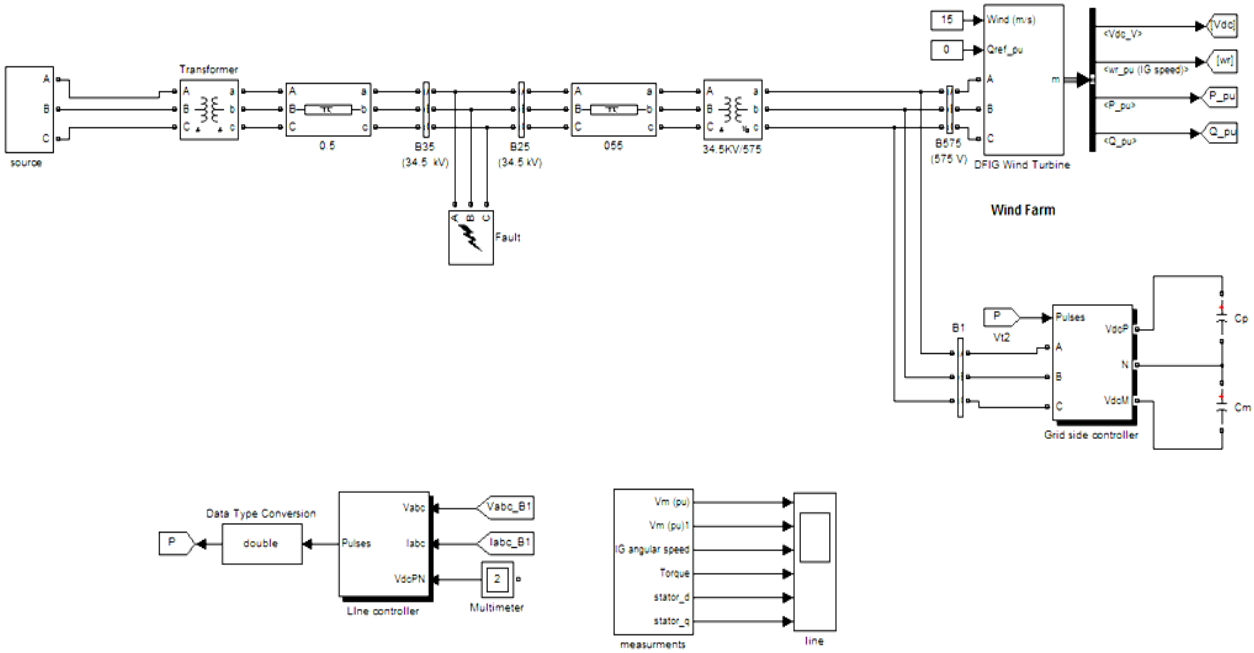

Figure 11. Simulation of the system under 2-phase fault without LVRT system

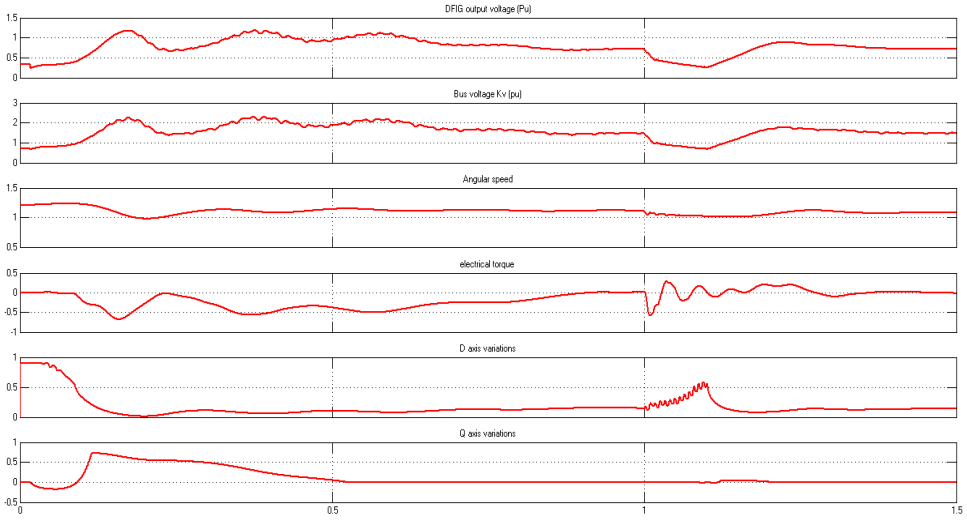

Figure 12. Waveform of the simulation for 2-phase fault without LVRT system

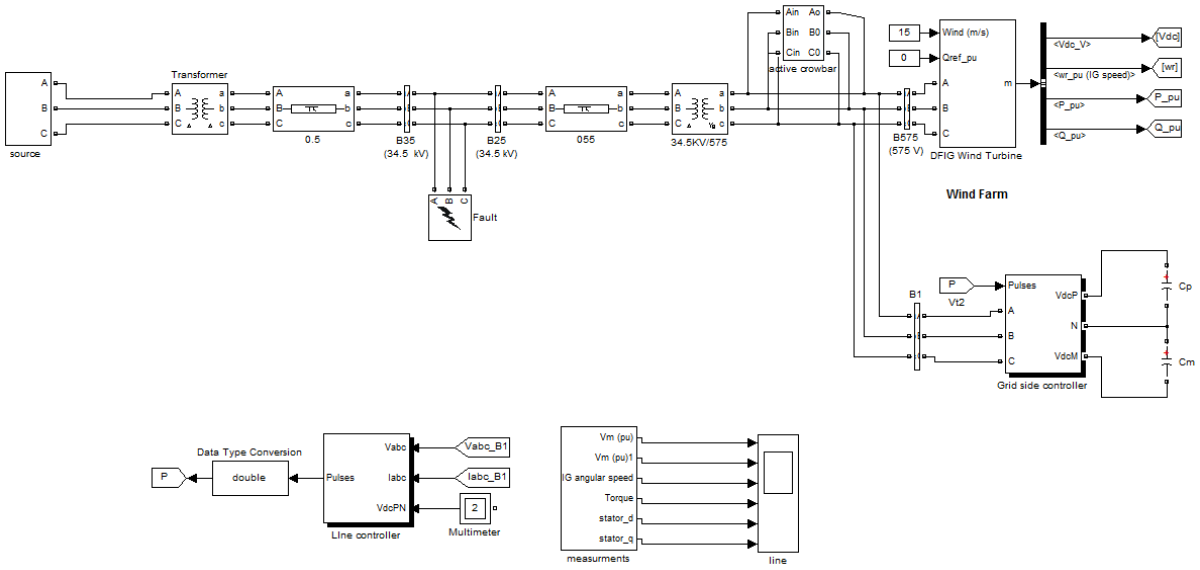

Figure 13. Simulation of the system under 2-phase fault with LVRT system

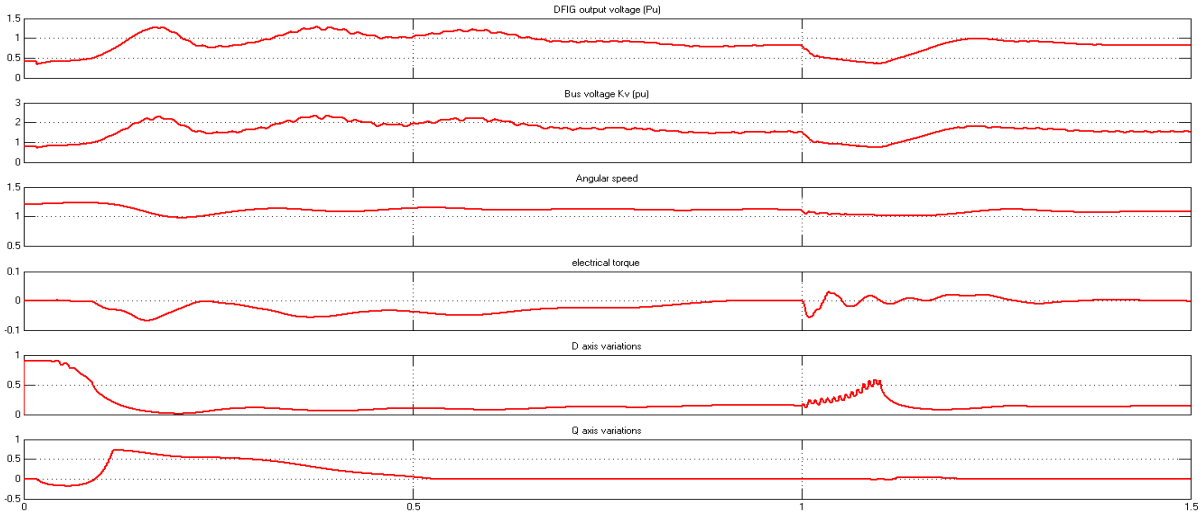

Figure 14. Waveform of the simulation for 2-phase fault with LVRT system

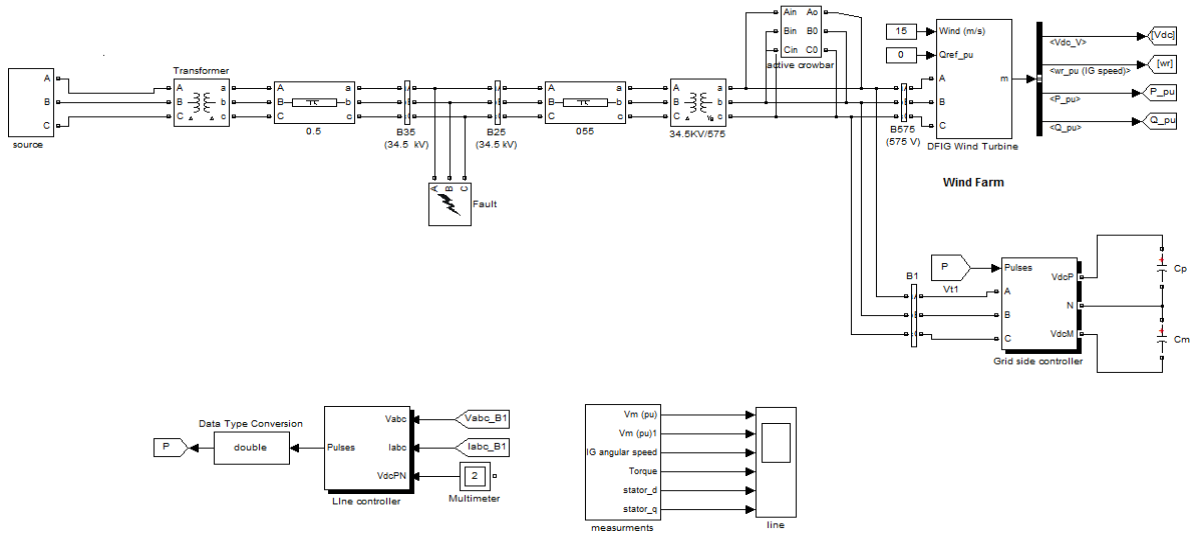

Figure 15. Simulation of the system under 2-phase fault with Fuzzy-LVRT system

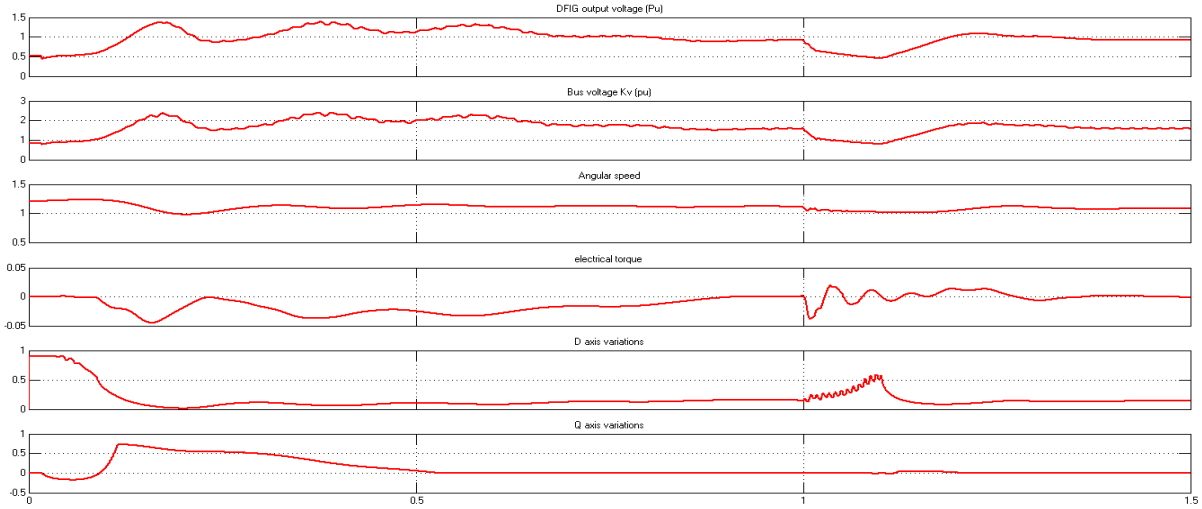

Figure 16. Waveform of the simulation for 2-phase fault with Fuzzy-LVRT system

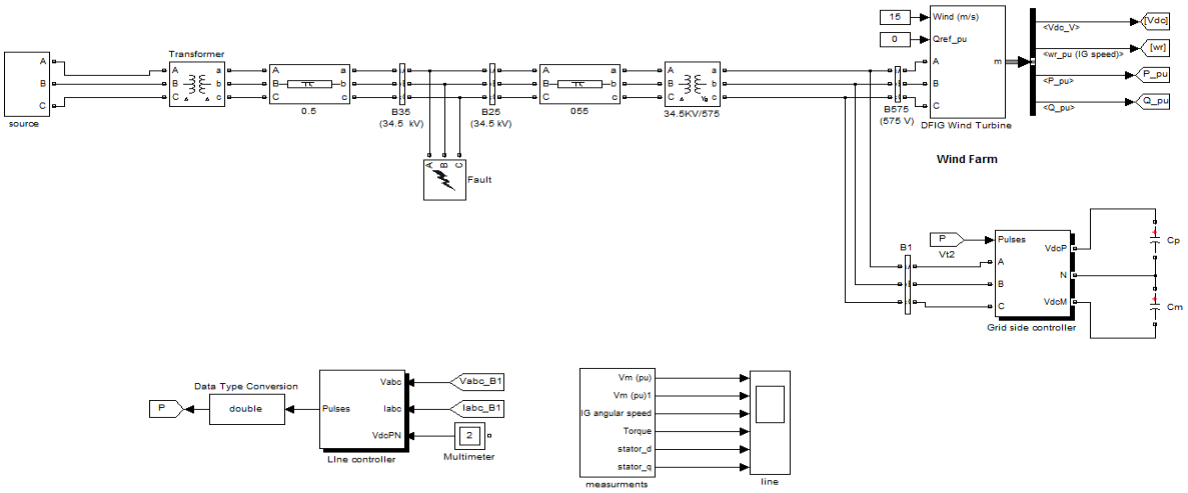

Figure 17. Simulation of the system under 3-phase fault without LVRT system

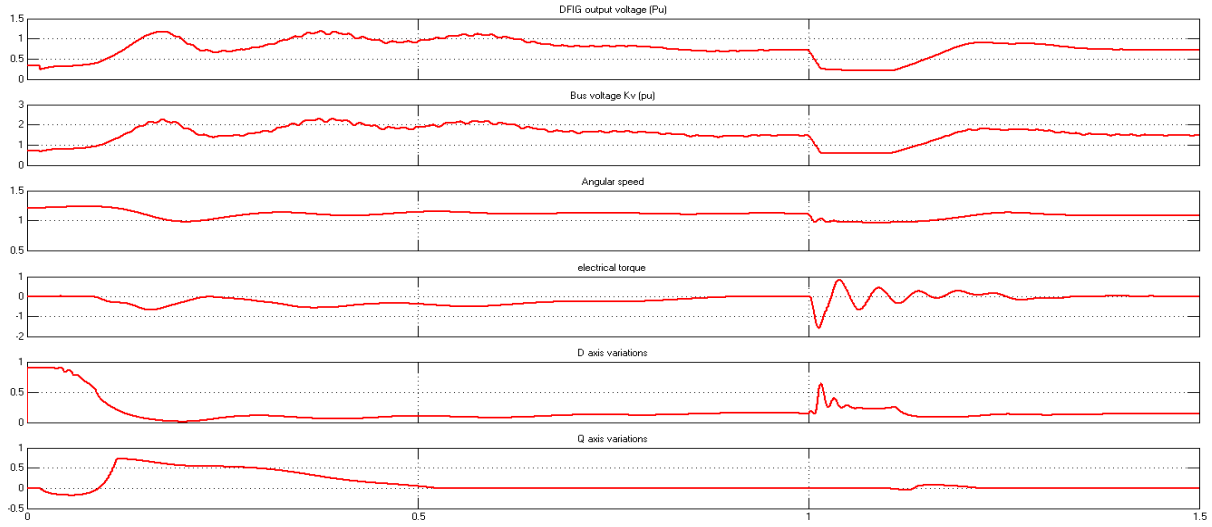

Figure 18. Waveform of the simulation for 3-phase fault without LVRT system

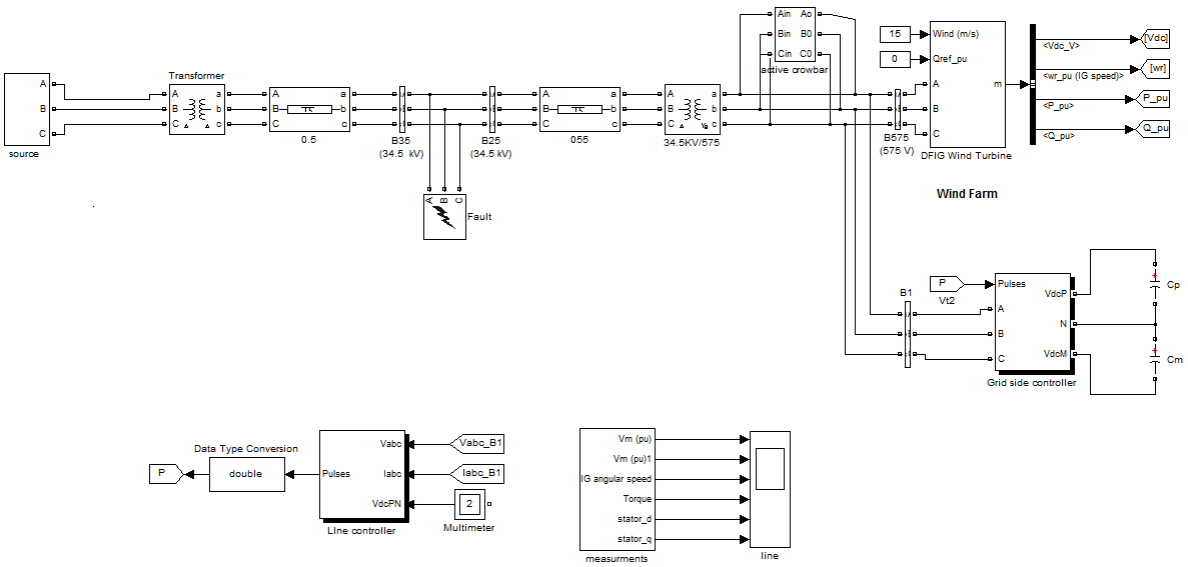

Figure 19. Simulation of the system under 3-phase fault with LVRT system

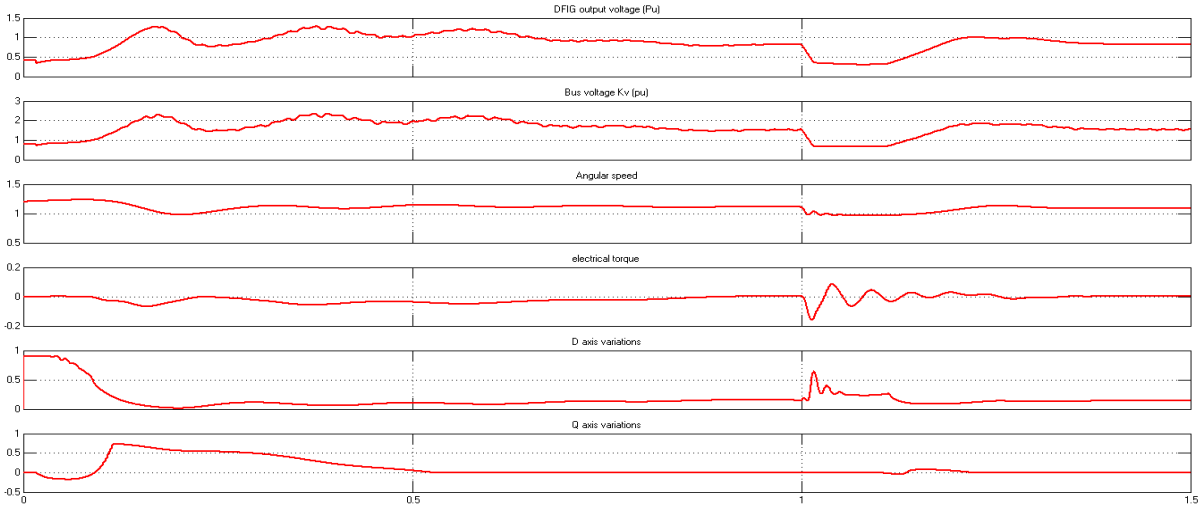

Figure 20. Simulation of the system under 3-phase fault with LVRT system

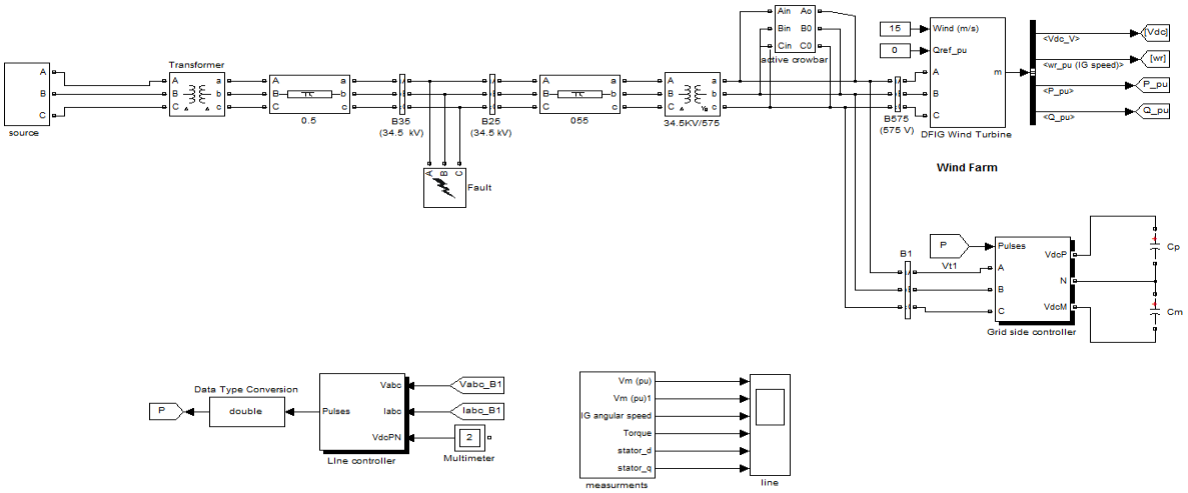

Figure 21. Simulation of the system under 3-phase fault with Fuzzy-LVRT system

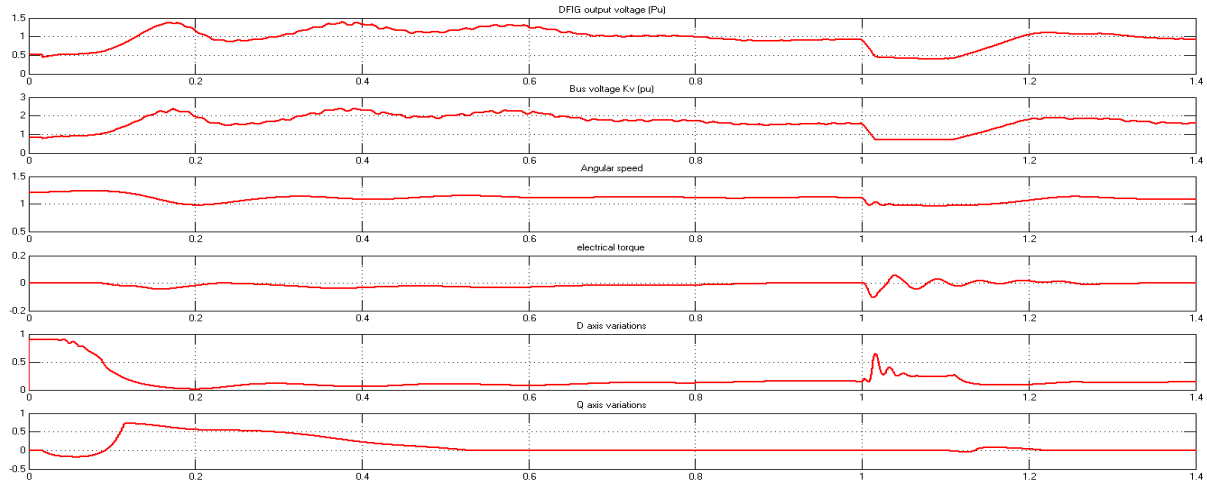

Figure 22. Waveform of the simulation for 3-phase fault with Fuzzy-LVRT system

Various parameters like bus voltage D-axis variation, DFIG output voltage, Q-axis variation, angular speed electrical torque are measured for 2-phase fault and 3-phase fault. The variation of each of them with respect to time is analyzed individually.

In addition, the variations of the parameter of the system with LVRT, with Fuzzy-LVRT and without LVRT are compared in the graph. Figure 23 shows the simulation of the system under 2-phase fault, using fuzzy logic controlled parallel resonance fault current limiter and the respective waveform is shown in Figure 24.

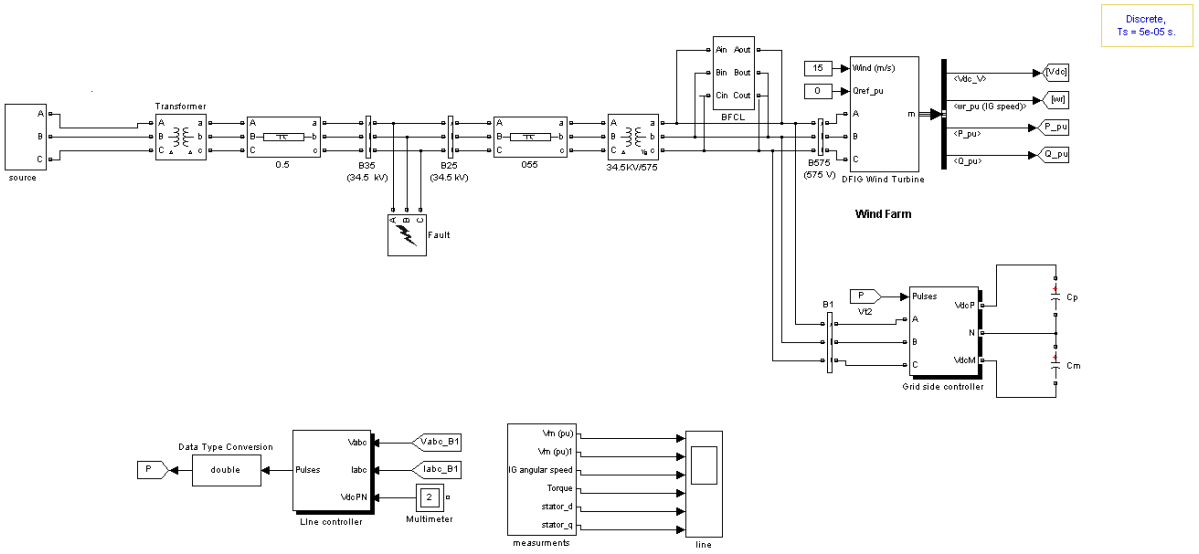

Figure 23. Simulation of the system under 2-phase fault with resonance fault current limiter system

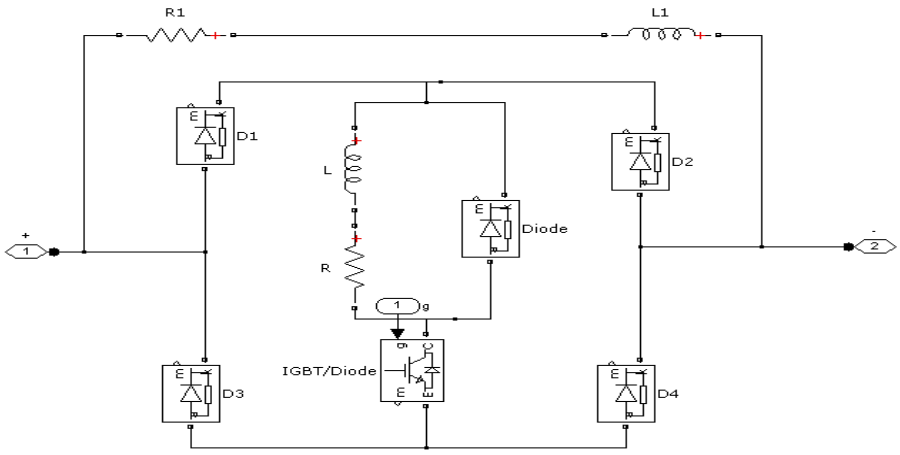

Figure 24. shows the simulation diagram of resonance fault current limiter system

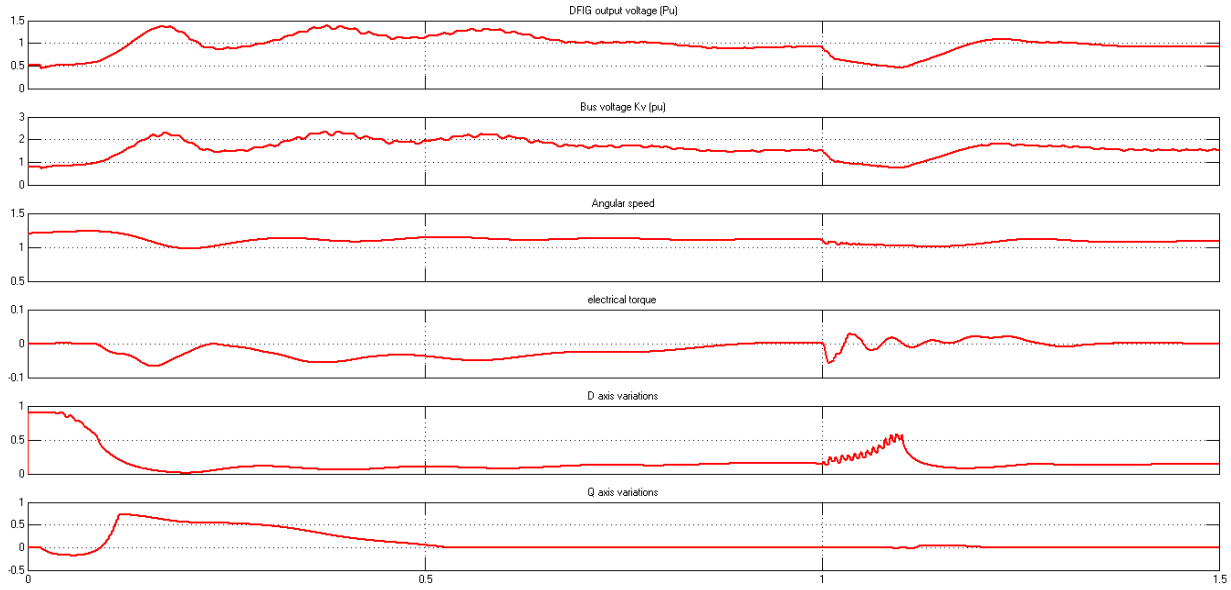

Figure 25. Waveform of the simulation for 2-phase fault with resonance fault current limiter system

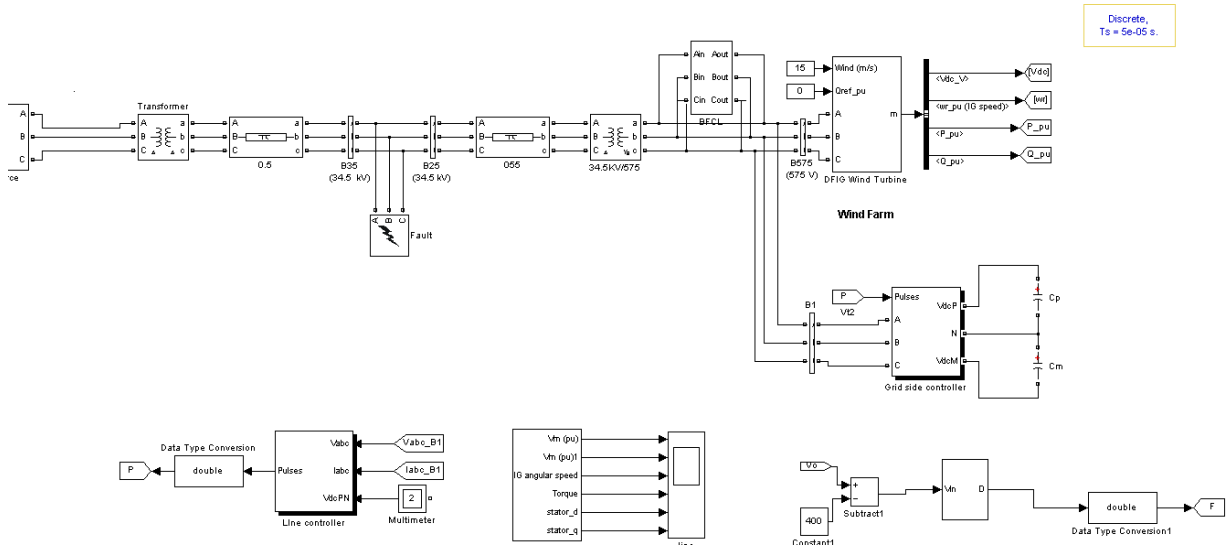

Figure 26. Simulation of the system under 2-phase fault with Fuzzy- resonance fault current limiter system

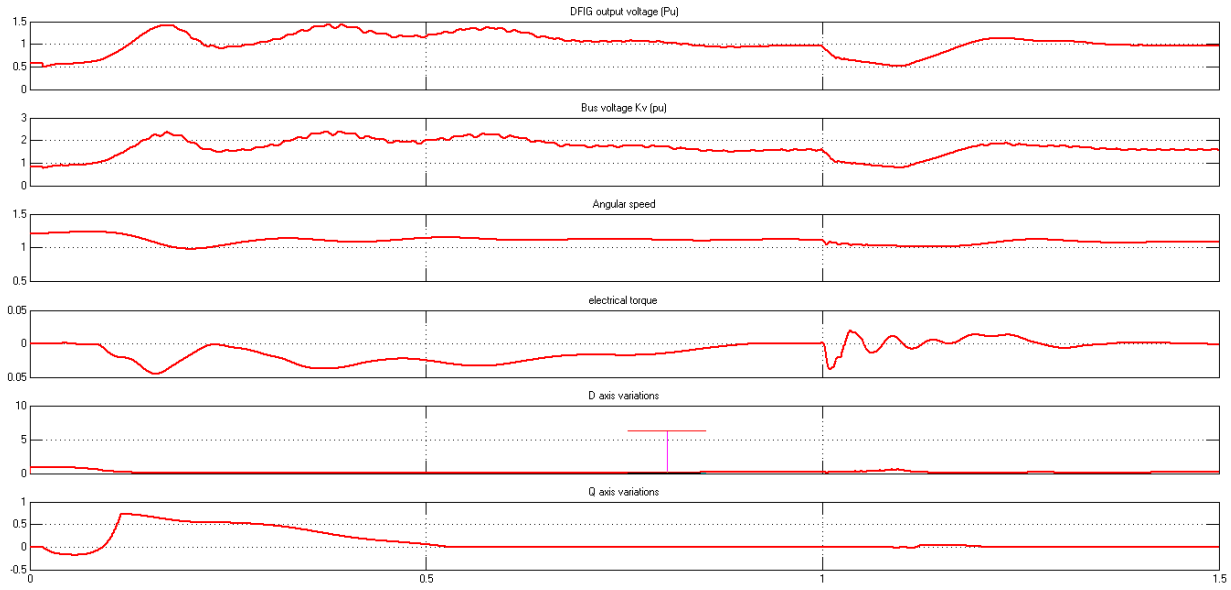

Figure 27. Waveform of the simulation for 2-phase fault with Fuzzy-resonance fault current limiter system

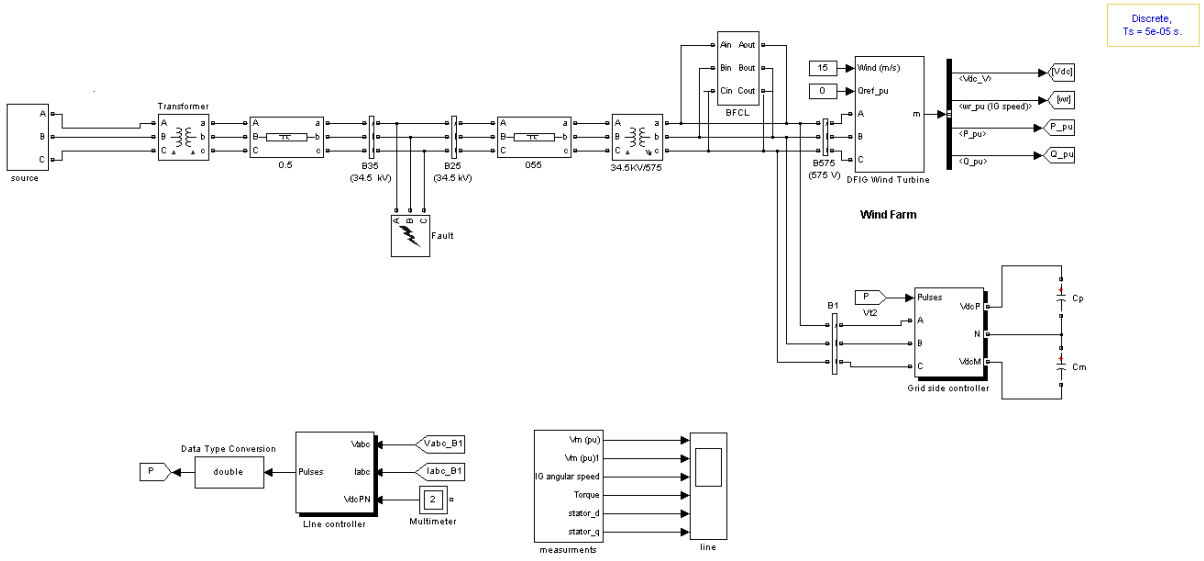

Figure 28. Simulation of the system under 3-phase fault with resonance fault current limiter system

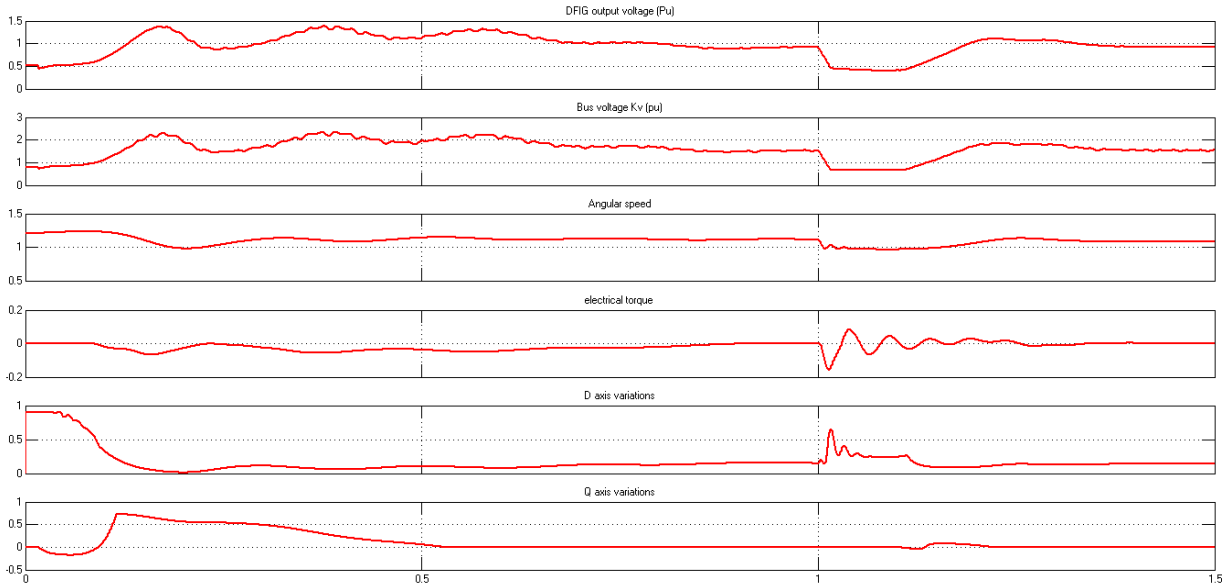

Figure 29. Waveform of the simulation for 3-phase fault with resonance fault current limiter system

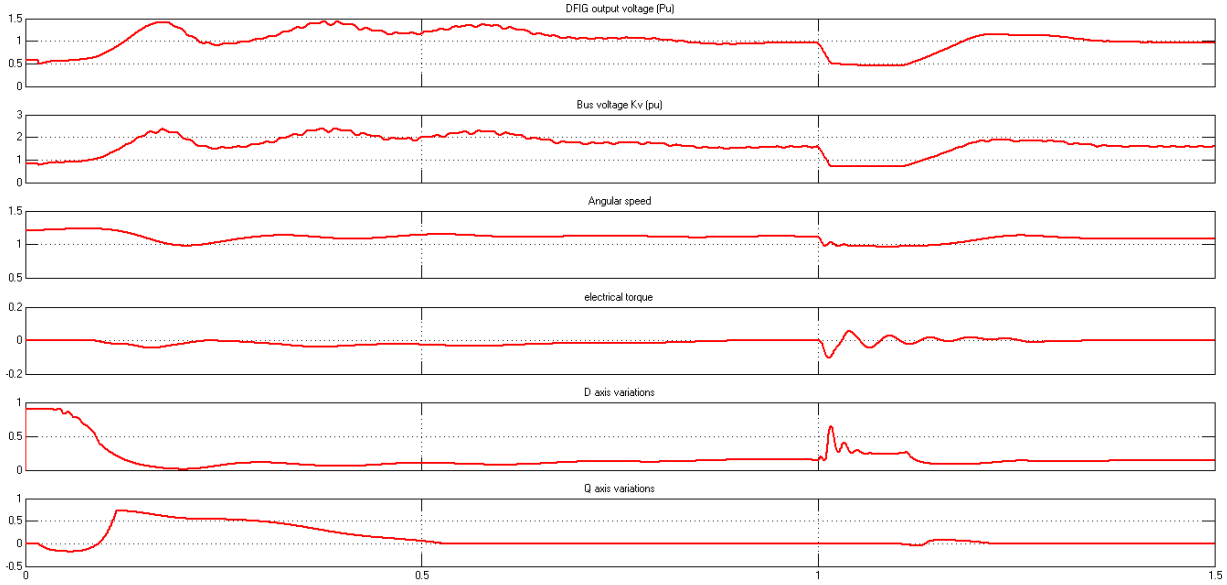

Figure 30. Waveform of the simulation for 3-phase fault with Fuzzy-resonance fault current limiter system

Figure 31 shows the variation of bus voltage for 2-phase fault, with respect to time. The bus voltage is shown in y-axis and observed between 0.8-2V, increased in the steps of 0.2V. Time is shown in x-axis from 0.9-1.4s increased in the steps of 0.05s. It is inferred from the graph that the Fuzzy-LVRT system attains the maximum bus voltage of 1.8V.In order to compare the effectiveness of the proposed fault current limiter a comparison of the three phases and the two phases are taken on the results it can be clearly stated that the regulation of the resonant limiter is far better as compared to the LVRT, adding the resonance conversion improves the system stability.

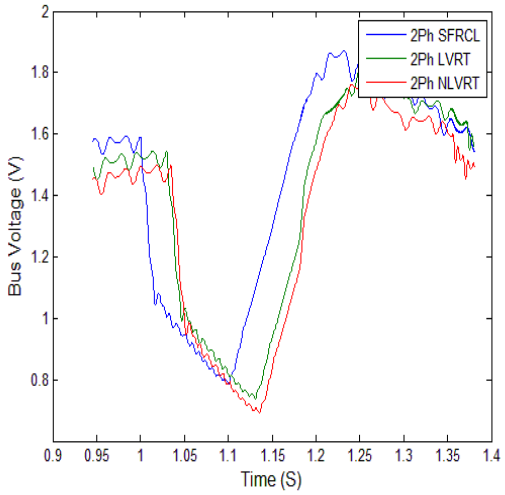

Figure 31. Bus voltage under 2-phase fault

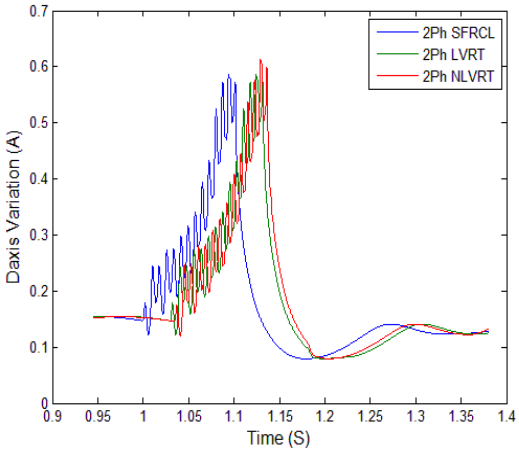

Figure 32. D-axis Variation under 2-phase fault

Figure 32 shows the D-axis Variation for 2-phase fault, with respect to time. The D-axis Variation is shown in y-axis, increased in the steps of 0.1A. Time is shown in x-axis from 0.9-1.4s increased in the steps of 0.05s. It is inferred from the graph that the Fuzzy-LVRT system attains less oscillations, starting at 1s. However, LVRT starts oscillating at 0.95s.

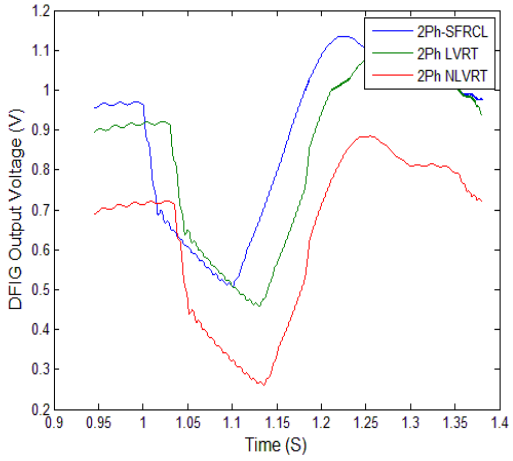

Figure 33. DFIG Output Voltage under 2-phase fault

Figure 33 shows DFIG Output Voltage for 2-phase fault, with respect to time. The DFIG Output Voltage is shown in y-axis and observed between 0.2-1.2V, increased in the steps of 0.1V. Time is shown in x-axis from 0.9-1.4s increased in the steps of 0.05s. It is inferred from the graph that the Fuzzy-LVRT system attains the maximum DFIG Output Voltage of 1.1V.

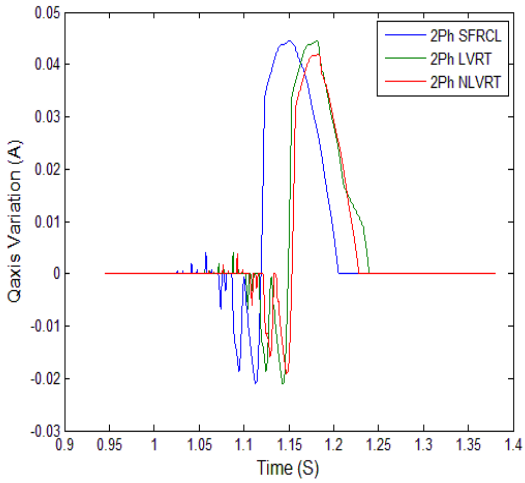

Figure 34. Q-axis Variation under 2-phase fault

Figure 34 shows Q-axis Variation for 2-phase fault, with respect to time. The Q-axis Variation is shown in y-axis and observed between -0.02-0.05A, increased in the steps of 0.01A. Time is shown in x-axis from 0.9-1.4s increased in the steps of 0.05s. It is inferred from the graph that the Fuzzy-LVRT system

attains lesser oscillations, starting at 1.05s. However, LVRT starts oscillating at 0.95s.

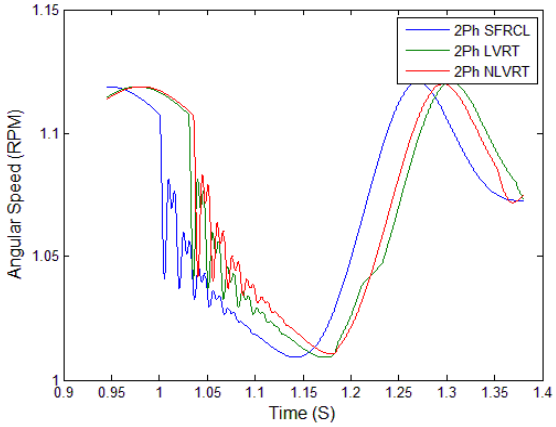

Figure 35. Angular Speed under 2-phase fault

Figure 35 shows the variation of angular Speed for phase fault, with respect to time. The Angular Speed is shown in y-axis and observed between 1-1.15 rpm, increased in the steps of 0.05rpm. Time is shown in x-axis from 0.9-1.4s increased in the steps of 0.05s. It is inferred from the graph that the Fuzzy-LVRT system attains the maximum Angular Speed.

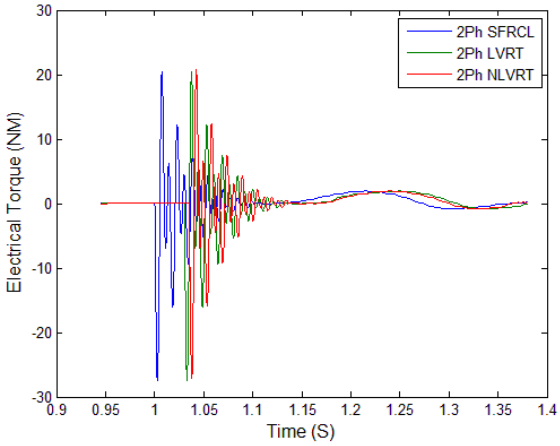

Figure 36. Electrical Torque under 2-phase fault

Table 2. Comparison of the performance of the resonant current limiting filter and the LVRT

	Without LVRT	**With LVRT**	**SFRCL**	**Variation %**	**Regulation**
DFIG voltage dip in Pu	0.25	0.42	0.68	1.61904762	0.26
Bus voltage in pu	0.75	0.82	0.91	1.1097561	0.09
Angular speed in pu	0.99	1.05	1.08	1.02857143	0.03
Electrical torque NM	-30	-25	-15	0.6	10
D axis variation A pu (peak)	0.65	0.61	0.55	0.90163934	-0.06
q Axis variation A pu (peak)	0.01	0.04	0.06	1.5	0.02

Figure 36 shows the variation Electrical Torque for 2-phase fault, with respect to time. The Electrical Torque is shown in y-axis and observed between -30-30Nm, increased in the steps of 10Nm. Time is shown in x-axis from 0.9-1.4s increased in the steps of 0.05s. The NLVRT oscillations are high compared to the variations of Fuzzy. Hence Fuzzy works better.

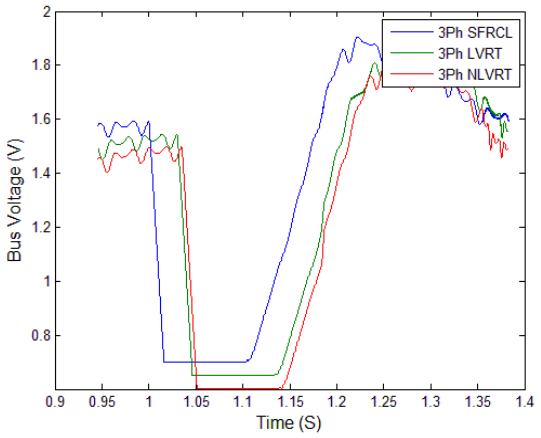

Figure 37. Bus voltage under 3-phase fault

Figure 37 shows the variation of bus voltage for 3-phase fault, with respect to time. The bus voltage is shown in y-axis and observed between 0.8-2V, increased in the steps of 0.2V. Time is shown in x-axis from 0.9-1.4s increased in the steps of 0.05s. It is inferred from the graph that the Fuzzy-LVRT system attains the maximum bus voltage.

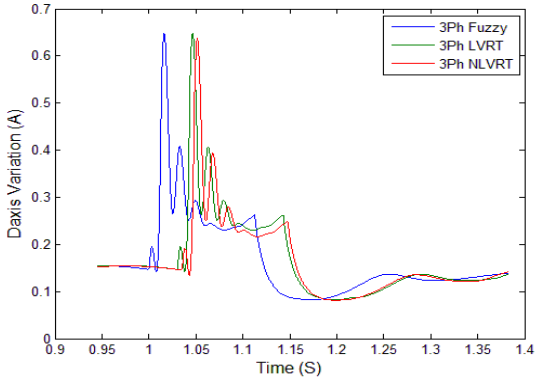

Figure 38. D-axis Variation under 3-phase fault

Figure 38 shows the D-axis Variation for 2-phase fault, with respect to time. The D-axis Variation is shown in y-axis, increased in the steps of 0.1A. Time is shown in x-axis from 0.9-1.4s increased in the steps of 0.05s. It is inferred from the graph that the Fuzzy-LVRT system attains less oscillations, starting at 1s. However, LVRT starts oscillating at 0.95s. The LVRT attains 0.63A variations. The NLVRT attains 0.61A variations. The fuzzy starts moving up and attains 0.65A. Out of three waveforms fuzzy attains the maximum limit.

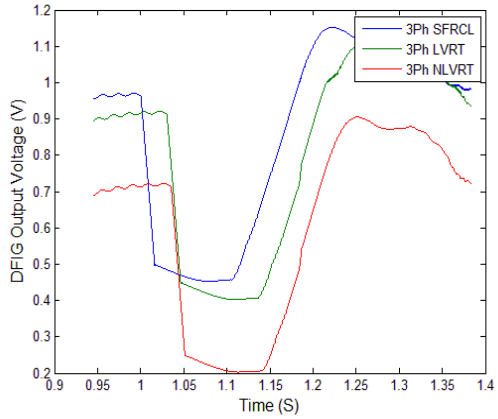

Figure 39. 3- DFIG Output Voltage(V) under 3-phase fault

Figure 39 shows DFIG Output Voltage for 3-phase fault, with respect to time. The DFIG Output Voltage is shown in y-axis and observed between 0.2-1.2V, increased in the steps of 0.1V. Time is shown in x-axis from 0.9-1.4s increased in the steps of 0.05s. The LVRT attains 0.3V. The NLVRT attains 0.2V variations. The Fuzzy starts moving down and attains 0.45V. Out of three waveforms fuzzy attains the maximum limit. It is inferred from the graph that the Fuzzy-LVRT system attains the maximum DFIG Output Voltage of 1.1V.

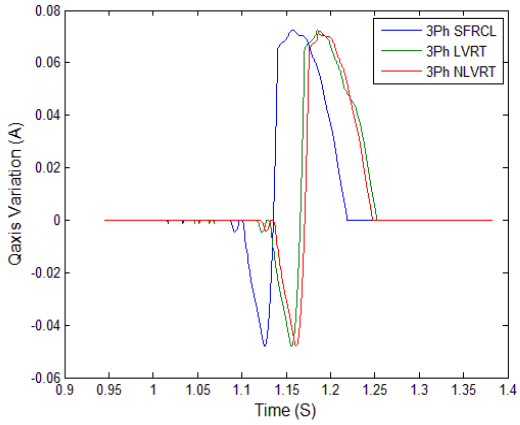

Figure 40. Q-axis variation(A) under 3-phase fault

Figure 40 shows Q-axis Variation for 3-phase fault, with respect to time. The Q-axis Variation is shown in y-axis and observed between -0.02-0.05A, increased in the steps of 0.01A. Time is shown in x-axis from 0.9-1.4s increased in the steps of 0.05s. The

LVRT variations attains 0.042A. The NLVRT attains 0.044A variations. The Fuzzy starts moving down and attains 0.045A variations. Out of three waveforms fuzzy attains the maximum limit. It is inferred from the graph that the Fuzzy-LVRT system attains lesser oscillations, starting at 1.05s. However, LVRT starts oscillating at 0.95s.

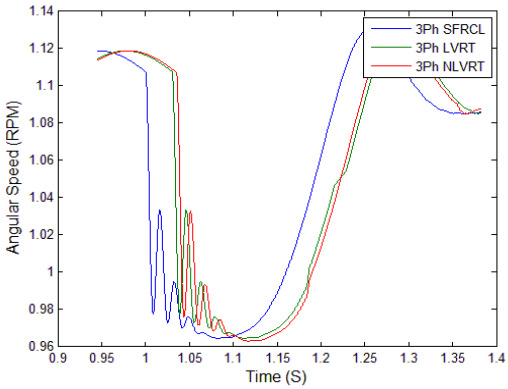

Figure 41. Angular speed(rpm) under 3-phase fault

Figure 41 shows the variation of angular Speed for 3-phase fault, with respect to time. The Angular Speed is shown in y-axis and observed between 0.96-1.14 rpm, increased in the steps of 0.02rpm. Time is shown in x-axis from 0.9-1.4s increased in the steps of 0.05s. It is inferred from the graph that the Fuzzy-LVRT system attains the maximum Angular Speed.

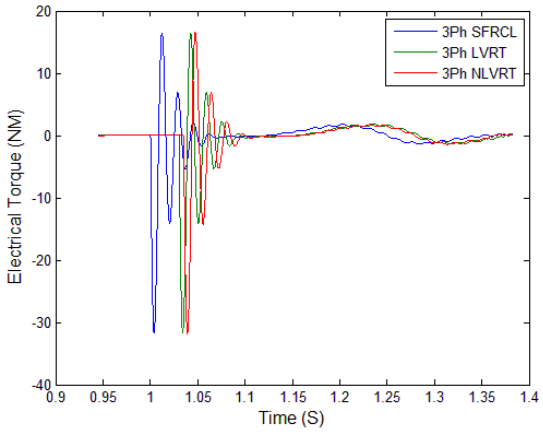

Figure 42. Electrical Torque under 3-phase fault

Figure 42 shows the variation Electrical Torque for 3-phase fault, with respect to time. The Electrical Torque is shown in y-axis and observed between -40-20Nm, increased in the steps of 10Nm. Time is shown in x-axis from 0.9-1.4s increased in the steps of 0.05s. The NLVRT oscillations are high compared to the variations of Fuzzy. Hence Fuzzy works better.

Table 3. Comparison of the 3 phase fault condition parameters of the DFIG

Parameters	Without LVRT	With LVRT	SFRCL	Variation %	Regulation
DFIG voltage dip in Pu	0.2	0.39	0.45	1.15384615	0.06
Bus voltage in pu	0.55	0.71	0.89	1.25352113	0.18
Angular speed in pu	0.96	0.97	0.98	1.01030928	0.01
Electrical torque NM	-25	-16	-10	0.625	6
D axis variation A pu (peak)	0.1	0.08	0.04	0.5	-0.04
q Axis variation A pu (peak)	0.01	0.04	0.06	1.5	0.02

Table 4. Comparison of the 3 and 2-phase phase fault condition parameters of the DFIG

Parameters	Without LVRT-2	Without LVRT=-3	With LVRT-2	With LVRT-2	SFRCL-3	SFRCL-3
DFIG voltage dip in Pu	0.25	0.2	0.42	0.39	0.68	0.45
Bus voltage in pu	0.75	0.55	0.82	0.71	0.91	0.89
Angular speed in pu	0.99	0.96	1.05	0.97	1.08	0.98
Electrical torque NM	-30	-25	-25	-16	-15	-10
D axis variation A pu (peak)	0.65	0.1	0.61	0.08	0.55	0.04
q Axis variation A pu (peak)	0.01	0.01	0.04	0.04	0.06	0.06

Table 5. Comparison of the variation and the control regulation parameters of the DFIG under both fault conditions

2-phase	Regulation	3-phase	Regulation
1.61905	0.26	1.15384615	0.06
1.10976	0.09	1.25352113	0.18
1.02857	0.03	1.01030928	0.01
0.6	10	0.625	6
0.90164	-0.06	0.5	-0.04
1.5	0.02	1.5	0.02

6 Conclusion

This study presents the implementation of an active LVRT for grid-integrated, DFIG-based wind farm. In the modeling of the DFIG, fuzzy logic controller and a parallel resonant filter were carried out together. A simpler model of DFIG with the parallel resonantfilter and balancing was ease computation. The transient behaviors of the system with and without the active LVRT were compared in terms of voltage dip, for a short duration.A 3-phase fault and a 2-phase fault were considered as transient stability conditions that might cause a low voltage dip at the grid. While increasing considerably in the 3-phase fault DFIG parameters, oscillation was lower in the 2-phase fault. It was found that the DFIG terminal voltage and 34.5 kV bus voltage increased by using an active LVRT capability during the fault. In comparison to the active and the passive LCRT schemes the FRT capability of a DFIG based wind farms can be enhanced significantly using the proposed fuzzy logic based parallel resonance filter for both symmetrical and asymmetrical faults since it operates as a nonlinear controller, the stable operation of the wind generator system is ensured than the crowbar circuits.Further the usefulness of the FLC-PRFCL on a system with distributed generation and grid-tied micro grid will be investigated.It outperforms the Crowbar, BFCL, and PI controlled

PRFCL. The FRT capability of a DFIG based wind farm can be enhanced for both symmetrical and asymmetrical faults. More stable operation of the DFIG based wind generator system will be ensured.

References:

[1] Liang J, Qiao W, Harley RG. Feed forward transient current control for low voltage ride through enhancement of DFIG wind turbines. IEEE Trans Energy Convers Vol.25, pp:836–43,2010.

[2] Liang J, Howard DF, Restrepo JA, Harley RG. Feed forward transient compensation control for DFIG wind turbines during both balanced and unbalanced grid disturbances. IEEE Trans Ind Appl, Vol.49, pp:1452–63,2013.

[3] Xiao S, Yang G, Zhou H, Geng H. An LVRT control strategy based on flux linkage tracking for DFIG-based WECS. IEEE Trans Ind Electron, Vol.60, pp:2820–32, 2013.

[4] Yang L, Xu Z, Ostergaard J, Dong ZY, Wong KP. Advanced control strategy of DFIG wind turbines for power system fault ride through. IEEE Trans Power Sys., Vol.27, pp:713–22.2012.

[5] Xie D, Xu Z, Yang L, Ostergaard J, Xue Y, Wong KP. A comprehensive LVRT control strategy for DFIG wind turbines with enhanced reactive power support, IEEE Trans Power Syst., Vol.28, pp:02–10, 2013.

[6] Lima FKA, Luna A, Rodriguez P, Watanabe EH, Blaabjerg F. Rotor voltage dynamics in the doubly fed induction generator during grid faults. IEEE Trans Power Electron., Vol.25, pp:118–30,2010.

[7] Mendes VF, de Sousa CV, Silva SR, Rabelo BC, Hofmann W. Modeling and ride through control of doubly fed induction generators during symmetrical voltage sags. IEEE Trans Energy Convers.,Vol. 26,pp:1161–71, 2011.

[8] Hossain MJ, Saha TK, Mithulananthan N, Pota HR. Control strategies for augmenting LVRT capability of DFIGs in interconnected power systems. IEEE Trans Ind Electron., Vol.60, pp:2510–22, 2013.

[9] Amuthan N, Subburaj P, Melba Mary P. Direct model reference adaptive internal model controller for better voltage sag ride through in doubly fed induction generator wind farms. Electrical Power Energy Syst.,Vol. 47,pp:255–63, 2013.

[10] Hu S, Lin X, Kang Y, Zou X. An improved low voltage ride through control strategy of doubly fed induction generators during grid faults. IEEE Trans Power Electron, Vol.26, pp:3653–65, 2011.

[11] Rahimi M, Parniani M. Grid fault ride through analysis and control of wind turbines with doubly fed induction generators. Electric Power Syst Res., Vol.80,pp:184–95,2010.

[12] Yao J, Li H, Liao Y, Chen Z. An improved control strategy of limiting the DC-link voltage fluctuation for a doubly fed induction wind generator. IEEE Trans Power Electron 2008;23:1205–13.

[13] Rahimi M, Parniani M. Coordinated control approaches for low voltage ride through enhancement in wind turbines with doubly fed induction generators. IEEE Trans Energy Convers., Vol.25,pp:873–83,2013.

[14] Wang D, Wang H, Jia J, Zhang Y. Reactive power control of doubly fed induction generator in wind farm under low grid voltage. In: 5th International Conference on Critical Infrastructure (CRIS 2010), Beijing; pp: 1–6,2010.

[15] Lopez J, Gubia E, Olea E, Ruiz J, Marroyo L. Ride through of wind turbines with doubly fed induction generator under symmetrical voltage dips. IEEE Trans Ind Electron., Vol.56,pp:4246–54,2009.

[16] Takahashi R, Tamura J, Futami M, Kimura M, Ide K. A new control method for wind energy conversion system using a double-fed synchronous generator. IEEJ Power and Energy, Vol.126, No.2,pp:225-235, 2006.

[17] Muyeen SM, Ali MH, Takahashi R, Murata T, Tamura J, Tomaki Y, et al. A comparative study on transient stability analysis of wind turbine generator system using different drive train models. IET Proc Renewab Power Gen.,Vol. 1, No.2, pp:131-141,2013.

[18] Muyeen SM, Takahashi R, Murata T, Tamura J. A variable speed wind turbine control strategy to meet wind farm grid code requirements. IEEE Trans Power Syst., Vol.25, No.1, pp:331-340, 2010.

[19] Erlich, Istvan, et al. Modeling of wind turbines based on doubly-fed induction generators for power system stability studies. IEEE Transactions on power systems, Vol.22, No.3,pp:909-919,2007.

[20] Morren, Johan, and Sjoerd WH De Haan. Ridethrough of wind turbines with doubly-fed induction generator during a voltage dip, IEEE Transactions on energy conversion, Vol.20, No.2 pp: 435-441,2005.